THE SAMI GALAXY SURVEY:
TOWARDS A UNIFIED DYNAMICAL SCALING RELATION FOR GALAXIES OF ALL TYPES

L. Cortese[1], L. M. R. Fogarty[2,3], I.-T. Ho[4], K. Bekki[5], J. Bland-Hawthorn[2,3], M. Colless[6], W. Couch[7], S. M. Croom[2,3], K. Glazebrook[1], J. Mould[1], N. Scott[2,3], R. Sharp[6], C. Tonini[8], J. T. Allen[2,3], J. Bloom[2,3], J. J. Bryant[2,3,7], M. Cluver[9], R. L. Davies[10], M. Drinkwater[11], M. Goodwin[7], A. Green[7], L. J. Kewley[6], I. S. Kostantopoulus[7,3], J. S. Lawrence[7], S. Mahajan[11,12], A. M. Medling[6], M. Owers[7], S. N. Richards[2,7,3], S. M. Sweet[6], O. I. Wong[5]

[1]Centre for Astrophysics & Supercomputing, Swinburne University of Technology, Hawthorn, 3122 Victoria, Australia
[2] Sydney Institute for Astronomy (SIfA), School of Physics, The University of Sydney, NSW 2006, Australia
[3] ARC Centre of Excellence for All-sky Astrophysics (CAASTRO)
[4] Institute for Astronomy, University of Hawaii, 2680 Woodlawn Drive, Honolulu, HI 96822, USA
[5] ICRAR, The University of Western Australia, Crawley WA 6009, Australia
[6] Research School of Astronomy & Astrophysics, The Australian National University, Cotter Road, Weston Creek, ACT 2611, Australia
[7] Australian Astronomical Observatory, PO Box 915, North Ryde, NSW 1670, Australia
[8] School of Physics, The University of Melbourne, VIC 3010, Australia
[9] Astronomy Department, University of Cape Town, Private Bag X3, Rondebosch7701, South Africa
[10] Astrophysics, Department of Physics, University of Oxford, Denys Wilkinson Building, Keble Rd., Oxford OX1 3RH, UK
[11] School of Mathematics and Physics, University of Queensland, QLD 4072, Australia
[12]Indian Institute of Science Education and Research Mohali-IISERM, Knowledge City, Sector 81, Manauli, PO 140306, India
Draft version September 2, 2014

ABSTRACT

We take advantage of the first data from the Sydney-AAO Multi-object Integral field (SAMI) Galaxy Survey to investigate the relation between the kinematics of gas and stars, and stellar mass in a comprehensive sample of nearby galaxies. We find that all 235 objects in our sample, regardless of their morphology, lie on a tight relation linking stellar mass (M_*) to internal velocity quantified by the $S_{0.5}$ parameter, which combines the contribution of both dispersion (σ) and rotational velocity (V_{rot}) to the dynamical support of a galaxy ($S_{0.5} = \sqrt{0.5V_{rot}^2 + \sigma^2}$). Our results are independent of the baryonic component from which σ and V_{rot} are estimated, as the $S_{0.5}$ of stars and gas agree remarkably well. This represents a significant improvement compared to the canonical M_* vs. V_{rot} and M_* vs. σ relations. Not only is no sample pruning necessary, but also stellar and gas kinematics can be used simultaneously, as the effect of asymmetric drift is taken into account once V_{rot} and σ are combined. Our findings illustrate how the combination of dispersion and rotational velocities for both gas and stars can provide us with a single dynamical scaling relation valid for galaxies of all morphologies across at least the stellar mass range 8.5< $log(M_*/M_\odot)$ <11. Such relation appears to be more general and at least as tight as any other dynamical scaling relation, representing a unique tool for investigating the link between galaxy kinematics and baryonic content, and a less biased comparison with theoretical models.

Subject headings: galaxies: evolution — galaxies: fundamental parameters — galaxies: kinematics and dynamics

1. INTRODUCTION

It is well established that the internal velocity of disk (Tully & Fisher 1977) and spheroidal galaxies (Faber & Jackson 1976) scales with their luminosity, stellar and baryonic mass (McGaugh et al. 2000). In addition to being important secondary distance indicators, the Tully-Fisher and Faber-Jackson relations provide strong constraints for understanding how galaxies form and evolve (e.g., Baugh 2006).

Unfortunately, both relations hold only for accurately pre-selected classes of objects (e.g., inclined disks and bulge-dominated systems, respectively), and their scatters and slopes vary when wider ranges of morphologies are considered (e.g., Neistein et al. 1999; Iodice et al. 2003; Williams et al. 2010; Catinella et al. 2012; Tonini et al. 2014). This limitation has hampered the comparison with theoretical models, as it is challenging to apply the same selection criteria used for observations to simulated data.

Thus, recent works have started investigating the possibility of bringing galaxies of all morphologies on the same dynamical scaling relation. Kassin et al. (2007) showed that, once the contributions of rotation (V_{rot}) and dispersion (σ) of the Hα-emitting gas are combined into the $S_{0.5}$ parameter ($S_{0.5} = \sqrt{0.5V_{rot}^2 + \sigma^2}$, Weiner et al. 2006), all star-forming galaxies (including merging systems) lie on a tight (∼0.1 dex scatter) stellar mass (M_*) vs. $S_{0.5}$ relation. Although it is still debated whether the combination of V_{rot} and σ is necessary to reduce the scatter in the Tully-Fisher relation of visually-classified disk galaxies (Miller et al. 2011), it is intriguing that the slope of the M_* vs. $S_{0.5}$ relation found by Kassin et al. (2007) is close to that of the Faber-Jackson relation, suggesting that a similar approach might hold also for quiescent systems.

Zaritsky et al. (2008) addressed this issue by using the $S_{0.5}$ parameter to show that ellipticals and disk galaxies lie on the same scaling relation. However, contrary to

Kassin et al. (2007) who directly combined σ and V_{rot}, they simply used rotational velocities for disks and integrated dispersion velocities for bulges. As in massive systems both rotation and dispersion contribute significantly to the dynamical support (Courteau et al. 2007; Emsellem et al. 2011), these assumptions cannot be generalised to the entire population of galaxies.

Catinella et al. (2012) was recently able to bring all massive ($M_* > 10^{10}$ M$_\odot$) galaxies on a tight relation by using the galaxy's concentration index to correct the stellar velocity dispersion of disk-dominated systems. This empirical approach is motivated by the observed dependence of the ratio of rotational to dispersion velocity on morphology (Courteau et al. 2007), suggesting that the $S_{0.5}$ parameter may indeed be applied to all types of galaxies.

In this Letter, we combine gas and stellar kinematics for 235 galaxies observed as part of the Sydney-AAO Multi-object Integral field (SAMI, Croom et al. 2012) Galaxy Survey (Bryant et al. 2014b) to show that *all* galaxies lie on the same M_* vs. $S_{0.5}$ relation. The major advantage of our approach lies in the measurement of dispersion and rotational velocities, from both stellar and gas components, from spatially resolved maps.

2. THE SAMI GALAXY SURVEY

The SAMI Galaxy Survey (Allen et al. 2014; Bryant et al. 2014b) is targeting ~3400 galaxies in the redshift range $0.004 < z < 0.095$ with the SAMI integral field unit, installed at the Anglo-Australian Telescope.

SAMI takes advantage of photonic imaging bundles ('hexabundles', Bland-Hawthorn et al. 2011; Bryant et al. 2014a) to simultaneously observe 12 galaxies across a 1 degree field of view. Each hexabundle is composed of 61 optical fibers, each with a diameter of ~1.6″, covering a total circular field of view of ~14.7″ in diameter. All SAMI fibers are fed into the AAOmega dual-beam spectrograph, providing a coverage of the 3700-5700 Å and 6250-7350 Å wavelength ranges at resolutions R~1750 and R~4500, respectively. These correspond to a full-width at half-maximum (FWHM) of ~170 km s^{-1} in the blue, and ~65 km s^{-1} in the red.

2.1. *Observations and data reduction*

We use the first 304 galaxies observed by SAMI in the footprint of the Galaxy And Mass Assembly Survey (GAMA, Driver et al. 2011). We focus on GAMA galaxies for the wealth of multiwavelength data available (see § 2.3).

Observations were carried out on March 5-17 and April 12-16, 2013. The typical observing strategy consists of seven dithered observations totalling 3.5 hours to achieve near-uniform spatial coverage across each hexabundle. The AAOmega data reduction pipeline 2DFDR was used to perform all the standard data reduction steps. Flux calibration was done taking advantage of a spectrophotometric standard star observed during the same night, while correction for telluric absorption was made using simultaneous observations of a secondary standard star (included in the same SAMI plate of the target). The row-stacked spectra of each exposure generated by 2DFDR were then combined, reconstructed into an image and resampled on a Cartesian grid of 0.5″×0.5″ spaxel size (see Sharp et al. 2014 and Allen et al. 2014 for more details on the flux calibration and resampling procedure).

2.2. *Stellar and gas kinematics*

To obtain homogenous global rotation and dispersion velocities for both gas and stars within one effective radius (r_e), we select the 250 galaxies in our sample with an r-band effective diameter (see § 2.3) smaller than the size of a SAMI hexabundle (14.7″), and greater than the typical spatial resolution of our observations (2.5″, i.e., ~2.1 kpc at the average redshift of our sample, see also Allen et al. 2014).

Stellar line-of-sight velocity and dispersion maps were then obtained using the penalised pixel-fitting routine PPXF, developed by Cappellari & Emsellem (2004), following the same technique described in Fogarty et al. (2014).

Gas velocity maps were created from the reduced data cubes using the new LZIFU IDL fitting routine (Ho et al. in prep.; see also Ho et al. 2014). After subtracting the stellar continuum with PPXF, LZIFU models the emission lines as Gaussians and performs a non-linear least-square fit using the Levenberg-Marquardt method. We fit up to 11 strong optical emission lines ([OII]$\lambda\lambda$3726,29, Hβ, [OIII]$\lambda\lambda$4959,5007, [OI]λ6300, [NII]$\lambda\lambda$6548,83, Hα, and [SII]$\lambda\lambda$6716,31) simultaneously, constraining all the lines to share the same rotation velocity and dispersion. Each line is modelled as a single-component Gaussian, and we use the reconstructed kinematic maps to measure gas rotation and velocity dispersion.

We then select our final sample as follows. First, spaxels are discarded if the fit failed or if the error on the velocities is greater than 20 km s^{-1} and 50 km s^{-1} for gas and stars, respectively. This conservative cut roughly corresponds to one third of spectral FWHM in SAMI cubes. Second, we estimate the fraction of 'good' spaxels (f) left within an ellipse of semi-major axis r_e and ellipticity and position angle determined from optical r-band Sloan Digital Sky Survey (SDSS, York et al. 2000) images (see § 2.3), and reject those galaxies with $f < 80\%$. This selection guarantees that we are properly tracing the galaxy kinematics up to r_e, and it leaves us with 235 individual galaxies: 193 with gas kinematics, 105 with stellar kinematics and 62 with both. Although our analysis takes advantage of less than 10% of the final SAMI Galaxy Survey, the sample size is already comparable to the largest IFU surveys of nearby galaxies to date (Cappellari et al. 2011; Sánchez et al. 2012).

Stellar and gas velocity widths (W) are obtained from the velocity histogram created by combining all the 'good' spaxels within r_e. Following the standard technique used for Hα rotation curves, we define W as the difference between the 90th and 10th percentile points of the velocity histogram ($W = V_{90} - V_{10}$, Catinella et al. 2005). We adopt the velocity histogram technique because this is the simplest method to determine velocity widths, making our results easily comparable to other studies, including long-slit spectroscopy. Rotational velocities are then computed as

$$V_{rot} = \frac{W}{2(1+z)sin(i)} \qquad (1)$$

where i is the galaxy inclination and z is the redshift.

Inclinations are determined from the r-band minor-to-major axis ratio (b/a) as:

$$cos(i) = \sqrt{\frac{(b/a)^2 - q_0^2}{1 - q_0^2}} \qquad (2)$$

where q_0 is the intrinsic axial ratio of an edge-on galaxy. Following Catinella et al. (2012), we adopt $q_0=0.2$ for all galaxies and set to inclination of 90 degrees if $b/a <0.2$. The average b/a of our sample is ~0.5.

Stellar and gas velocity dispersions are defined as the linear average of the velocity dispersion measured in each 'good' spaxel. We preferred linear to luminosity-weighted averages to be consistent with our velocity width measurements (which are not luminosity-weighted) and because these are less affected by beam smearing (Davies et al. 2011). Our conclusions, however, are unchanged if we use luminosity-weighted quantities. Excluding the effect of inclination, we assume a conservative uncertainty of 0.1 dex in the estimate of both V_{rot} and σ.

Finally, we combine dispersion and rotation through the S_K parameter:

$$S_K = \sqrt{KV_{rot}^2 + \sigma^2} \qquad (3)$$

As discussed in Weiner et al. (2006) and Kassin et al. (2007), this quantity includes the dynamical support from both ordered and disordered motions and, thus, should be a better proxy for the global velocity of the galactic halo. Moreover, it is almost unaffected by beam smearing, as the artificial increase of σ and decrease of V_{rot} compensate each other once they are combined into S_K (Covington et al. 2010).

Although the value of K varies with the properties of the system, in this paper we follow the simple approach of Kassin et al. (2007) and Zaritsky et al. (2008), and fix $K=0.5$. Our conclusions do not change for $0.3< K <1$.

2.3. *Ancillary data*

The SAMI data are combined with multiwavelength observations obtained as part of the GAMA survey. Briefly, r-band effective radii, position angles and ellipticities are taken from the one-component Sersic fits presented in Kelvin et al. (2012)[1]. Stellar masses (M_*) are estimated from $g - i$ colours and i-band magnitudes following Taylor et al. (2011, see also Bryant et al. 2014b).

Visual morphological classification has been performed on the SDSS colour images, following the scheme used by Kelvin et al. (2014). Galaxies are first divided into late- and early-types according to their shape, presence of spiral arms and/or signs of star formation. Then, early-types with just a bulge are classified as ellipticals (E), whereas those with disks as S0s. Similarly, late-type galaxies with a bulge component are Sa-Sb, whereas bulge-less late-type galaxies are Sc or later.

3. DYNAMICAL SCALING RELATIONS

In Fig. 1 we show M_* vs. V_{rot} (left panel), σ (middle) and $S_{0.5}$ (right) for all 235 galaxies in our sample. Circles and triangles indicate galaxies with kinematical parameters from stellar and gas components, respectively. Thus, the 62 galaxies for which both gas and stellar kinematics are available appear twice in each plot. In the bottom row, galaxies are colour-coded according to their morphology.

3.1. *The stellar mass Tully-Fisher relation*

Our M_* vs. V_{rot} relation has a larger scatter (~0.22 dex in V_{rot} from the inverse fit)[2] than classical Tully-Fisher relations (~0.08 dex). This is not surprising as our sample includes early-types and face-on systems that would normally be excluded from Tully-Fisher studies (e.g., Catinella et al. 2012). Indeed, as shown in Fig. 1d, a significant fraction of the scatter is due to spirals with bulges, and early types.

The M_* vs. V_{rot} relation for the stars (circles) is significantly offset from the one of the gas (triangles): i.e., at fixed M_*, stars rotate slower than gas. This is clearer in Fig. 2a, where we compare V_{rot} of gas and stars for the 62 galaxies with both measurements available. Once galaxies with clear misalignments between gas and stellar rotation axis are excluded (empty circles), we find that V_{rot}(gas) is, on average, ~0.14 dex (with standard deviation $SD \sim0.11$ dex) higher than V_{rot}(stars). This is a consequence of asymmetric drift: while gas and stars experience the same galactic potential, a larger part of the stellar dynamical support comes from dispersion. The average ratio V_{rot}(stars)$/V_{rot}$(gas) is 0.75 ($SD \sim0.20$), roughly $\sim20\%$ lower than the value obtained by Martinsson et al. (2013) by comparing the maximum rotational velocities of pure disk galaxies (V_{rot}(stars)$/V_{rot}$(gas)~0.89). This is likely due to the fact that we are probing only the central parts of galaxies, where asymmetric drift is more prominent.

For comparison, in Fig. 1a,d, we show the local stellar mass Tully-Fisher relation (Bell & de Jong 2001)[3]. Our relation is significantly flatter, showing a good match only at high stellar masses. This is again because our rotational velocities are measured within one r_e. As the rotation curves of giant galaxies rise more quickly than in dwarfs (Catinella et al. 2006), our V_{rot} are close to the maximum rotational velocity only in massive systems (see also Fig. 2 in Yegorova & Salucci 2007).

3.2. *The stellar mass Faber-Jackson relation*

As for the M_* vs. V_{rot} relation, the scatter of our M_* vs. σ relation is significantly larger (~0.17 dex) than the one typically obtained for early-type galaxies only (~0.07 dex, Gallazzi et al. 2006). As shown by Catinella et al. (2012), we find that the offset from the M_* vs. σ(stars) relation for early-type galaxies (Gallazzi et al. 2006; dashed line) correlates with the concentration index $[\Delta\sigma(\text{stars}) = (-0.41\pm0.07) + (0.14\pm0.03) \times (R_{90}/R_{50})]$. This confirms that, at fixed M_*, disks are more rotationally supported than bulge-dominated systems.

---

[1] We re-computed the ellipticity and position angle for seven galaxies with bright bars or other issues (GAMA 250277, 279818, 296685, 383259, 419632, 536625, 618152) as the published values do not match the orientation of the velocity field.

[2] All scatters in this paper are estimated from the inverse linear fit along the x-axis.

[3] Stellar masses have been converted to a Chabrier Initial Mass Function following Gallazzi et al. (2008).
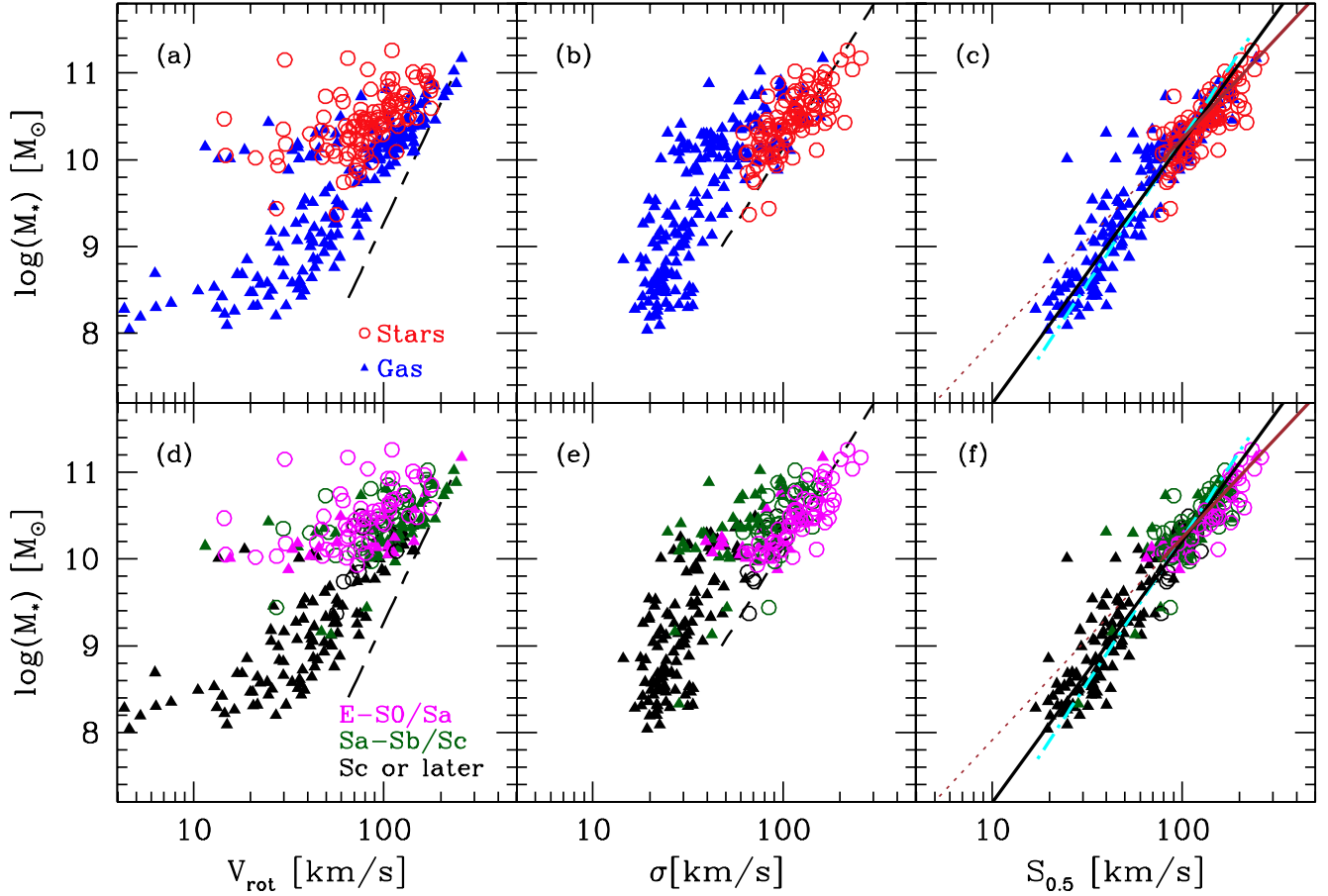
Figure 1. The M_* vs. V_{rot} (left), σ (center) and $S_{0.5}$ (right) relations for our SAMI sample. Circles and triangles indicate stellar and gas kinematics, respectively. In the bottom row, symbols are colour-coded according to morphological type: E-S0/Sa (magenta), Sa-Sb/Sc (dark green), Sc or later types (black). The stellar mass Tully-Fisher (Bell & de Jong 2001, long-short dashed line) and Faber-Jackson (Gallazzi et al. 2006, dashed line) relations for nearby galaxies are shown in the left and central panel for comparison. In the right panels, the best inverse linear fit for the whole sample, and for $M_* > 10^{10}$ M$_\odot$ are indicated by the black and brown solid lines, respectively. The dashed-dotted line shows the M_* vs. $S_{0.5}$ relation obtained by Kassin et al. (2007).
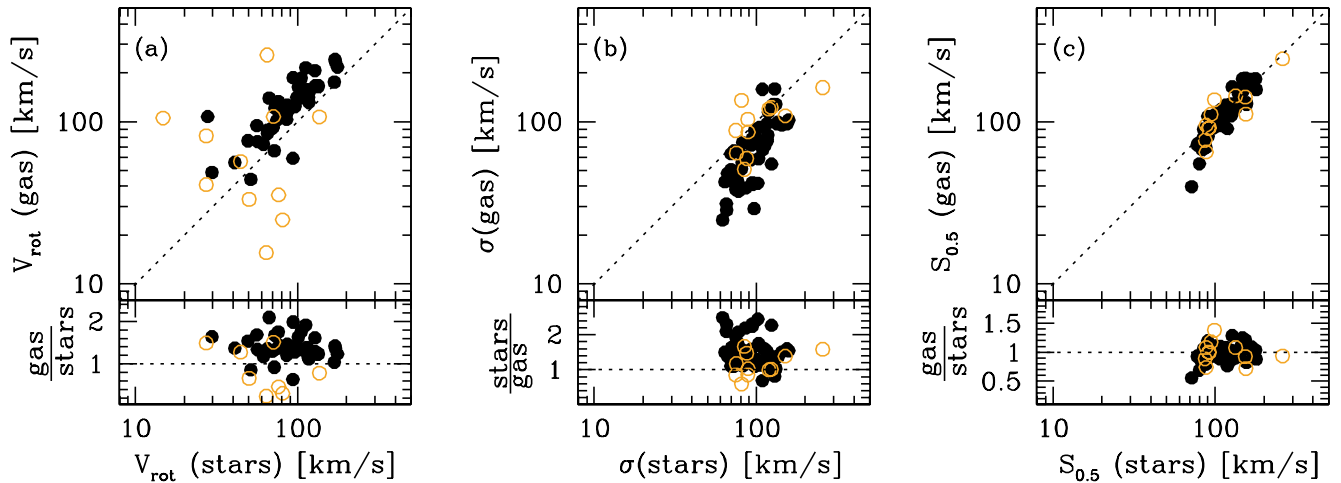
Figure 2. Comparison between rotation (V_{rot}, left), dispersion velocities (σ, center) and $S_{0.5}$ (right) of gas and stars, for the 62 galaxies in our sample with both measurements available. Empty circles highlight galaxies where gas and stars have a misaligned rotation axis. In each panel, the dotted line shows the 1-to-1 relation.

Even in this case, the scaling relations of stars and gas are offset, with σ(gas) on average 0.17 dex ($SD \sim$0.13 dex) lower than σ(stars) (Fig. 2b; see also Ho 2009). In addition, the M_* vs. σ relation for the gas shows a clear break at $M_* \sim 10^{10}$ $M_\odot$, with smaller galaxies having roughly the same velocity dispersion ($\sim$30 km s^{-1}), i.e., the typical value observed in pure disk galaxies (Epinat et al. 2008).

3.3. The M_* vs. $S_{0.5}$ relation

The large scatter and the difference between stars and gas observed for the M_* vs. σ and M_* vs. V_{rot} relations disappear when V_{rot} and σ are combined in the $S_{0.5}$ parameter (see Fig. 1c,f). All morphological types follow the same scaling relation with small scatter and just a few outliers. An inverse linear fit (assuming $S_{0.5}$ as dependent variable) gives a scatter of $\sim$0.1 dex (solid line in Fig. 1c,f)[4]. The slope and intercept of the linear relation (0.33±0.01, −1.39±0.08) are similar to what is found by Kassin et al. (2007) for a sample of nearby star-forming galaxies with Hα rotation curves (dotted-dashed line). This is interesting, as Kassin et al. (2007) used maximum rotational velocities.

The remarkable agreement between the $S_{0.5}$ for gas and stars is shown in Fig. 2c: the average logarithmic difference (gas-stars) is just ~ -0.02 dex ($SD \sim 0.07$dex), even including disturbed galaxies. This is expected if both quantities trace the potential of the galaxy, and justifies their combination on the same scaling relation. The agreement between gas and stars is little affected by the value of K used to combine V_{rot} and σ. Indeed, the average logarithmic difference varies between -0.05 and $+0.03$ dex for $0.3 < K < 1$, and SD stays roughly the same.

Fig. 2 confirms that the reduced scatter in the M_* vs. $S_{0.5}$ relation is not simply a 'numerical artefact' due to the fact that we are linearly combining two quantities in a log-log plot. Indeed, gas and stars are brought on the same scaling relation only once the effect of asymmetric drift is properly taken into account.

Finally, we note that the M_* vs. $S_{0.5}$ relation may become steeper for $M_* < 10^{10}$ $M_\odot$. Indeed, if we only fit massive galaxies (solid brown line in Fig. 1c,f, with its extrapolation indicated as dotted line), low-mass systems are systematically below the relation: i.e., at fixed $S_{0.5}$ their stellar mass is lower than predicted from the extrapolation of the fit.

This break might simply reflect the one observed in the M_* vs. σ relation, but it interesting to note that a similar feature is also typically observed in the stellar mass Tully-Fisher relation of pure disk galaxies (Mc-Gaugh et al. 2000), and disappears in its baryonic version, which accounts for the mass of cold gas in galaxies. Unfortunately, the absence of cold gas measurements makes it impossible to compute a baryonic $S_{0.5}$ relation. Here we simply note that, if we use the ultraviolet and optical properties of our systems to predict their total gas content[5], the residuals from the linear fit correlate with
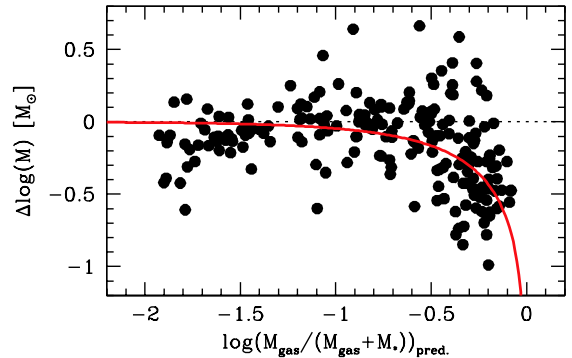
Figure 3. Residual along the y-axis (M_*) of the best fitting M_* vs. $S_{0.5}$ relation for massive galaxies ($M_* > 10^{10}$ $M_\odot$) as a function of 'predicted' gas fraction (see text for details). The red line is the trend expected if $S_{0.5}$ linearly correlates with total baryon mass.

the total gas fraction (Fig. 3) roughly as expected if the $S_{0.5}$ correlates linearly with total *baryonic* mass (red line in Fig. 3). However, given all the assumptions, the idea that a linear baryonic $S_{0.5}$ relation might be a fundamental physical relation linking galaxies of all types, remains for the time being just an intriguing speculation.

4. CONCLUSIONS

In this paper we take advantage of the first large statistical sample observed by the SAMI Galaxy Survey to show that all galaxies, regardless of their morphology, follow a tight ($\sim$0.1 dex) dynamical scaling relation once their dynamical support is expressed by combining the contributions of both rotational and dispersion velocities. We highlight that, while the stellar and gas components show systematic differences in their rotational and dispersion velocities (mainly due to the effect of asymmetric drift), their $S_{0.5}$ agree remarkably well. This justifies the simultaneous use of both gas and stellar kinematical indicators, allowing us to bring both star-forming and quiescent systems on the same physical relation.

Our analysis improves on Kassin et al. (2007) by showing that quiescent objects follow the same M_* vs. $S_{0.5}$ relation as star-forming systems. To our knowledge, this is the first time that gas and stellar rotational and dispersion velocities for galaxies of all morphological types are combined on the same dynamical scaling relation. This is a significant step forward compared to Zaritsky et al. (2008), and it shows that the $S_{0.5}$ parameter can be applied to all types of galaxies. In addition, we present evidence for a possible change in the slope of the M_* vs. $S_{0.5}$ relation at low stellar masses.

The $S_{0.5}$ parameter works remarkably well not only because it combines the contributions of both rotation and dispersion to the dynamical support of galaxies, but also because it is influenced only weakly by instrumental effects (Covington et al. 2010). While here we use K=0.5, our main conclusions remain unchanged for $0.3 < K < 1$.

Finally, it is important to remember that, as already known for the Tully-Fisher and Faber-Jackson relations, we can expect that the slope and scatter of the M_* vs. $S_{0.5}$ relation may depend on the technique used to estimate V_{rot} and σ, as well as on the radius at which both quantities are measured. We plan to investigate

---

[4] Note that galaxies with both $S_{0.5}$(gas) and $S_{0.5}$(stars) do not contribute twice to the fit, as for these we use the average between the two values.

[5] Atomic hydrogen masses are estimated from $NUV - r$ colours and stellar mass surface densities following Cortese et al. (2011).

Total gas fractions are then obtained assuming a molecular-to-atomic gas ratio of 0.3 (Boselli et al. 2014) and a helium contribution of 30%

this further in the future with the full SAMI sample, as determining the best combination of rotational and dispersion velocity should reveal important information on the kinematical structure of galaxies.

In the meantime, it is clear that the absence of any pre-selection in the sample not only makes the $S_{0.5}$ parameter extremely promising for characterising the dynamical properties of galaxies, but also might allow a more rigorous comparison with theoretical models.

REFERENCES

Allen, J. T., Croom, S. M., Baldry, I. K., et al. 2014, MNRAS submitted
Baugh, C. M. 2006, Reports on Progress in Physics, 69, 3101
Bell, E. F. & de Jong, R. S. 2001, ApJ, 550, 212
Bland-Hawthorn, J., Bryant, J., Robertson, G., et al. 2011, Optics Express, 19, 2649
Boselli, A., Cortese, L., Boquien, M., et al. 2014, A&A, 564, A66
Bryant, J. J., Bland-Hawthorn, J., Fogarty, L. M. R., Lawrence, J. S., & Croom, S. M. 2014a, MNRAS, 438, 869
Bryant, J. J., Owers, M., Robotham, A., et al. 2014b, MNRAS submitted
Cappellari, M. & Emsellem, E. 2004, PASP, 116, 138
Cappellari, M., Emsellem, E., Krajnović, D., et al. 2011, MNRAS, 413, 813
Catinella, B., Giovanelli, R., & Haynes, M. P. 2006, ApJ, 640, 751
Catinella, B., Haynes, M. P., & Giovanelli, R. 2005, AJ, 130, 1037
Catinella, B., Kauffmann, G., Schiminovich, D., et al. 2012, MNRAS, 420, 1959
Cortese, L., Catinella, B., Boissier, S., Boselli, A., & Heinis, S. 2011, MNRAS, 415, 1797
Courteau, S., McDonald, M., Widrow, L. M., & Holtzman, J. 2007, ApJ, 655, L21
Covington, M. D., Kassin, S. A., Dutton, A. A., et al. 2010, ApJ, 710, 279
Croom, S. M., Lawrence, J. S., Bland-Hawthorn, J., et al. 2012, MNRAS, 421, 872
Davies, R., Förster Schreiber, N. M., Cresci, G., et al. 2011, ApJ, 741, 69
Driver, S. P., Hill, D. T., Kelvin, L. S., et al. 2011, MNRAS, 413, 971
Emsellem, E., Cappellari, M., Krajnović, D., et al. 2011, MNRAS, 414, 888
Epinat, B., Amram, P., Marcelin, M., et al. 2008, MNRAS, 388, 500
Faber, S. M. & Jackson, R. E. 1976, ApJ, 204, 668
Fogarty, L. M. R., Scott, N., Owers, M. S., et al. 2014, MNRAS, 443, 485
Gallazzi, A., Brinchmann, J., Charlot, S., & White, S. D. M. 2008, MNRAS, 383, 1439
Gallazzi, A., Charlot, S., Brinchmann, J., & White, S. D. M. 2006, MNRAS, 370, 1106
Ho, I., Kewley, L. J., Dopita, M. A., et al. 2014, MNRAS in press (arXiv:1407.2411)
Ho, L. C. 2009, ApJ, 699, 638
Iodice, E., Arnaboldi, M., Bournaud, F., et al. 2003, ApJ, 585, 730
Kassin, S. A., Weiner, B. J., Faber, S. M., et al. 2007, ApJ, 660, L35
Kelvin, L. S., Driver, S. P., Robotham, A. S. G., et al. 2014, MNRAS, 439, 1245
Kelvin, L. S., Driver, S. P., Robotham, A. S. G., et al. 2012, MNRAS, 421, 1007
Martinsson, T. P. K., Verheijen, M. A. W., Westfall, K. B., et al. 2013, A&A, 557, A130
McGaugh, S. S., Schombert, J. M., Bothun, G. D., & de Blok, W. J. G. 2000, ApJ, 533, L99
Miller, S. H., Bundy, K., Sullivan, M., Ellis, R. S., & Treu, T. 2011, ApJ, 741, 115
Neistein, E., Maoz, D., Rix, H.-W., & Tonry, J. L. 1999, AJ, 117, 2666
Sánchez, S. F., Kennicutt, R. C., Gil de Paz, A., et al. 2012, A&A, 538, A8
Sharp, R., Allen, J. T., Fogarty, L. M. R., et al. 2014, MNRAS submitted
Taylor, E. N., Hopkins, A. M., Baldry, I. K., et al. 2011, MNRAS, 418, 1587
Tonini, C., Jones, D. H., Mould, J., et al. 2014, MNRAS, 438, 3332
Tully, R. B. & Fisher, J. R. 1977, A&A, 54, 661
Weiner, B. J., Willmer, C. N. A., Faber, S. M., et al. 2006, ApJ, 653, 1027
Williams, M. J., Bureau, M., & Cappellari, M. 2010, MNRAS, 409, 1330
Yegorova, I. A. & Salucci, P. 2007, MNRAS, 377, 507
York, D. G., Adelman, J., Anderson, Jr., J. E., et al. 2000, AJ, 120, 1579
Zaritsky, D., Zabludoff, A. I., & Gonzalez, A. H. 2008, ApJ, 682, 68